S & M 4197

Molecular Dynamics Simulation of Mechanical Characteristics of Nanoscale Iron Particles during Laser Powder Bed Fusion Additive Manufacturing

Ling-Feng Lai, ¹ Deng-Maw Lu, ¹ Chih-Liang Chu, ¹ and Jian-Ming Lu^{2*}

 Department of Mechanical Engineering, Southern Taiwan University of Science and Technology, Number 1, Nan-tai Street, Yungkang District, Tainan City 710301, Taiwan
 Department of AI UAS Technology, Wufeng University, 117, Sec. 2, Chiankuo Rd., Minhsiung, Chiayi County 621303, Taiwan

(Received March 31, 2025; accepted October 1, 2025)

Keywords: molecular dynamics, particle, additive manufacturing, coalescence temperature, melting temperature

A simulation method with the embedded atom model (EAM)/alloy potential energy function was used to determine the mechanical characteristics of nanoscale spherical solid and hollow iron (Fe) particles of various sizes under different laser heating rates during laser powder bed fusion (PBF) additive manufacturing (AM). We concluded that the coalescence temperatures of nanoscale spherical solid and hollow Fe particles were in the range from 1300 to 1732 K and from 1150 to 1682 K, respectively. We found that the macroscopic melting point of Fe (1811 K) was much greater than the melting temperatures of nanoscale spherical solid and hollow Fe particles. We also found that the melting temperatures of nanoscale spherical solid and hollow Fe particles were in the ranges from 1600 to 1785 K and from 1515 to 1767 K, respectively. We found that the interdiffusion of Fe atoms slows down while the heating rate increases. The solidstate sintering of nanoscale spherical solid and hollow Fe particles can readily take place at room temperature (300 K). We found that the interdiffusion of Fe atoms slows down while the heating rate increases. The solid-state sintering of nanoscale spherical solid and hollow Fe particles can also spontaneously occur at room temperature (300 K). The sizes and geometrical microstructures of nanoscale particles and laser heating rates are important factors during laser PBF AM.

1. Introduction

In 2009, the American Society for Testing and Materials classified additive manufacturing (AM) technologies⁽¹⁻⁷⁾ into seven categories. Among them, metallic AM technologies were divided into four categories, namely, powder bed fusion (PBF),⁽¹⁻⁴⁾ direct energy deposition,⁽⁵⁾ binder jetting,⁽⁶⁾ and sheet lamination.⁽⁷⁾ The materials, microstructure, and mechanical behaviors are the important parameters of AM technologies. With computer-aided design

^{*}Corresponding author: e-mail: jmlu@wfu.edu.tw https://doi.org/10.18494/SAM5676

software, the design concepts are drawn into 3D prototypes, and AM parameters such as temperature, heating rate, number of 3D printing layers, support structures, and printing speed are also important. AM technologies have been extensively used in, for example, nanosensors, microsensors, surface coating, architecture, art, aerospace, machines, and biomedicine. The geometrical microstructures of metallic nanoparticles and microparticles obtained by the above AM technologies have different sizes and geometrical shapes. Fe is one of the transition elements and accounts for a considerable proportion in the Earth's crust, mantle, and core. In addition, Fe is inexpensive and has high hardness and good ductility; thus, it is mostly made into forms such as carbon steel, stainless steel, and alloy steel. Fe^(8,9) is also utilized in such products as jewelry, spark plugs, catalytic converters, gas sensors, surgical instruments, and dental implants. We determined the mechanical characteristics of nanoscale spherical solid and hollow Fe particles, and the optimal parameters under different sizes and laser heating rates during laser PBF AM were also found.

2. Materials and Methods

2.1 Molecular dynamics (MD) simulations

MD^(10–14) was derived from Newtonian mechanics, and MD with a suitable potential energy function is able to simulate the motion of the atomic positions, atomic trajectories, and atomic interforces of Fe nanoparticles. The large-scale atomic/molecular massively parallel simulator (LAMMPS)^(15–19) is one of the open-source MD simulation programs. In this work, LAMMPS was used to simulate the microstructures, thermodynamic behaviors, and interforces of nanoscale spherical solid and hollow Fe particles, as well as to investigate their mechanical properties, coalescence temperatures, and melting temperatures.

2.2 Atomic model preparation

2.2.1 Spherical nanoscale solid particles

In this study, nanoscale spherical solid and hollow Fe particles were simulated using LAMMPS. The nonperiodic boundary conditions and the canonical ensemble, which represent the system in thermal equilibrium at a fixed temperature, were used, and the initial microstructure of nanoscale Fe particles was the body-centered cubic (BCC) crystal structure. The space of the simulation box was several times larger than that of nanoscale solid and hollow Fe particles. The initial gap between the nanoscale Fe particles was set to 5 Å, and the sizes of the Fe particles were 16a, 20a, and 24a. Table 1 lists 12 Fe nanoparticles sizes with two identical and different sizes, and Fig. 1 shows the cross-sectional views of nanoscale solid and hollow Fe particles.

e	Structure	D1	D2	# Atoms
1	Solid nanoscale particle pairs	16a	16a	8570
2		20a	20a	16786
3		24a	24a	28722
4		16a	20a	12678
5		16a	24a	18646
6		20a	24a	22754
7	Hollow nanoscale particle pairs	16a	16a	7496
8		20a	20a	13112
9		24a	24a	20152
10		16a	20a	10304
11		16a	24a	13824
12		20a	24a	16632

Table 1
Parameters and number of atoms (#Atoms) in nanoscale spherical Fe particle pairs

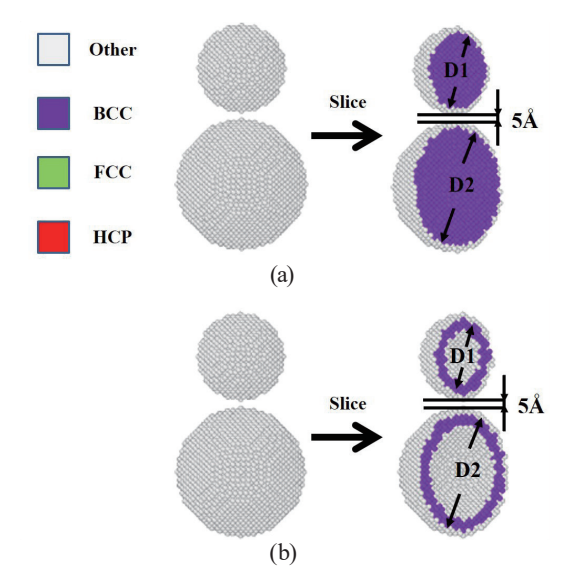


Fig. 1. (Color online) Cross-sectional views of nanoscale spherical Fe particles: (a) solid model and (b) hollow model.

2.2.2 Nanoscale spherical hollow particles

First, in order to simulate hollow Fe particles, the middle part of the nanoscale spherical solid Fe particle needs to be removed to obtain a nanoscale spherical hollow Fe particle with the shell thickness of 4 Å with a gap of 5 Å. The remaining arguments and particle sizes are the same as shown in Table 1 and Fig. 1.

2.3 Auxiliary analysis and calculation

2.3.1 Common neighbor analysis (CNA)

 ${\rm CNA^{(20)}}$ can simulate spherical solid and hollow Fe nanoparticles in laser PBF AM and visualize each lattice structure at each time step.

2.3.2 Gyration radius

Gyration radius $(R_g)^{(21)}$ was used to calculate the mean square distance (MSD) between each Fe atom and the center of mass of nanoscale spherical solid and hollow Fe particles during laser PBF AM. The total mass of the system is M, the center of mass of the system is at r_{cm} , the position of each Fe atom is r, and the subscript i represents all the Fe atoms in the system. (22)

$$R_g^2 = \frac{1}{M} \sum_{i} m_i \left(r_i - r_{cm} \right)^2 \tag{1}$$

2.3.3 Mean square displacement

MSD can be used to simulate the trajectories of Fe atoms in nanoscale spherical solid and hollow Fe particles during laser PBF AM. MSD is the average distance between Fe atoms. The total mass of the system is N and the time is t.⁽²³⁾

$$MSD = \frac{1}{N} \sum_{i} [r_i(t) - r_i(0)]^2$$
 (2)

3. Results and Analysis

3.1 Nanoscale spherical solid particles

3.1.1 Thermal equilibration at room temperature (300 K)

LAMMPS was used to simulate nanoscale spherical solid Fe particles. During laser PBF AM, the internal lattice microstructures, neck widths, interaction forces, trajectories, and disordered atoms were investigated at room temperature (300 K). The four points a, b, c, and d in Fig. 2 correspond to the four substates (a), (b), (c), and (d), respectively. At Point a, the initial gap

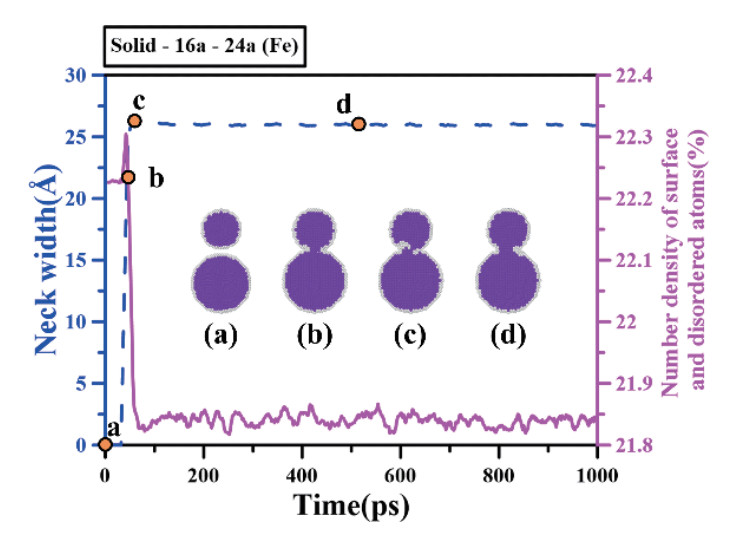


Fig. 2. (Color online) Nanoscale spherical solid Fe particles of the combination 16a–24a in Table 1. Time histories of neck width and number density of surface and disordered atoms for the solid Fe nanoparticle pair are shown.

of 5 Å between nanoscale spherical solid Fe particles was maintained, R_g was 35.90 Å, and the neck width was 0 Å. The BCC crystal structure accounted for 77.78%, the hexagonal close-packed (HCP) crystal structure accounted for 0%, the face-centered cubic (FCC) crystal structure accounted for 0%, and other structures accounted for 22.22% of substate (a). The small size effect at Point b caused the nanoscale spherical solid Fe particles to coalesce together. R_g was 35.89 Å, the neck width was 23.94 Å, BCC accounted for 77.81%, HCP and FCC accounted for 0%, and other structures accounted for 22.19% of substate (b). Owing to the high proportion of disordered atoms in the spherical solid Fe nanoparticles, R_g was 35.88 Å, the neck width was 25.46 Å, BCC accounted for 77.60%, HCP and FCC accounted for 0%, and other structures accounted for 22.40% of substate (c). The internal crystal structures of nanoscale spherical solid Fe particles were in equilibrium, R_g was 35.86 Å, neck width was 25.99 Å, BCC accounted for 78.19%, HCP and FCC accounted for 0%, and other structures accounted for 21.81% of substate (d).

3.1.2 Sintering

The crystal structures of nanoscale spherical solid Fe particles produced during laser PBF AM were investigated by CNA using LAMMPS with the embedded atom model (EAM)/alloy potential. The proportions of BCC, FCC, HCP, and disordered atoms in the nanoscale spherical solid Fe particles were also calculated. Moreover, the position, trajectory, and R_g of Fe atoms of nanoscale spherical solid Fe particles were calculated at each time step during laser PBF AM. In Fig. 3, nanoscale spherical solid Fe particles were laser-heated at 1 K/ps and divided into four sections by Points A, B, C, D, and E. Nanoscale spherical solid Fe particles were relatively stable between Points A and C. The range from Points C to D corresponds to the coalescence temperature of nanoscale spherical solid Fe particles. Nanoscale spherical solid Fe particles gradually melted from Points D to E, and the internal lattice structure changed considerably.

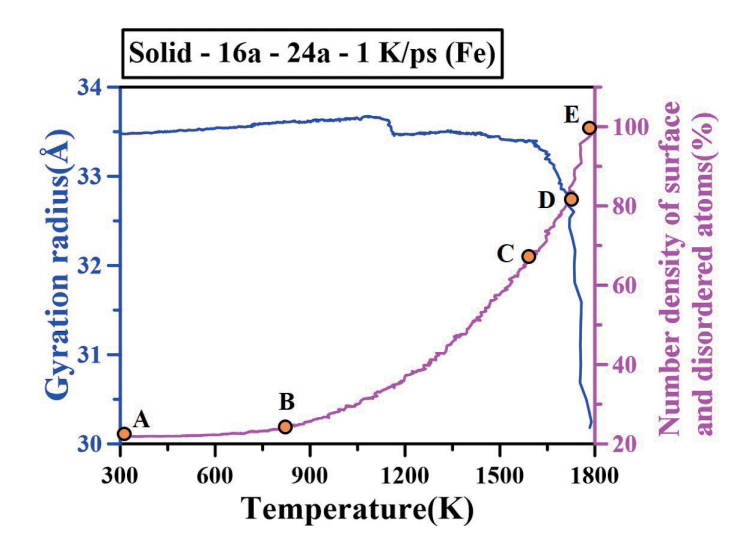


Fig. 3. (Color online) Nanoscale spherical solid Fe particles of the combination 16a-24a from Table 1 were sintered in the range from 300 to 1800 K at 1 K/ps. The variation of the number density of atomic surface and disordered Fe atoms and R_g is shown.

Nanoscale spherical solid Fe particles completely melted beyond Point E. In Fig. 4, nanoscale spherical solid Fe particles were linearly heated at heating rates of 1, 0.5, and 0.25 K/ps during the laser PBF AM. We found that the MSD of the internal Fe atoms of nanoscale spherical solid Fe particles at 0.25 K/ps was the largest, and the diffusion behaviors of those at 0.25 K/ps were the best. At 1 K/ps, the diffusion temperature started at 1162 K, and the diffusion MSD was 339 Ų. At 0.5 K/ps, the diffusion temperature started at 1100 K, and the diffusion MSD was 550 Ų. At 0.25 K/ps, the diffusion temperature started at 1040 K, and the diffusion MSD was 850 Ų. The starting diffusion temperature of nanoscale spherical solid Fe particles at 1 K/ps was from 1162 to 1250 K, and the diffusion RMS was from 218 to 450 Ų. The starting diffusion temperature at 0.5 K/ps was from 1089 to 1170 K, and the diffusion MSD was from 550 to 685 Ų. The starting diffusion temperature at 0.25 K/ps was from 1030 to 1100 K, and the diffusion MSD was from 850 to 1050 Ų. Using the cutoff radius and potential energy function in Figs. 5 and 6, it was found that the coalescence temperatures of nanoscale spherical solid Fe particles during laser PBF AM were from 1300 to 1732 K and the melting temperatures were from 1600 to 1785 K.

3.2 Nanoscale spherical hollow particles

3.2.1 Thermal equilibration at 300 K

During laser PBF AM, CNA was performed using LAMMPS with the EAM/alloy potential to investigate the crystal structures of nanoscale spherical hollow Fe particles at room temperature (300 K). The proportions of BCC, FCC, HCP, and disordered atoms in the nanoscale spherical hollow Fe particles were also calculated. Also, the internal lattice structures, neck widths, interaction forces, positions, trajectories, disordered atoms, and R_g of Fe atoms of nanoscale hollow Fe particles were calculated at each time step.

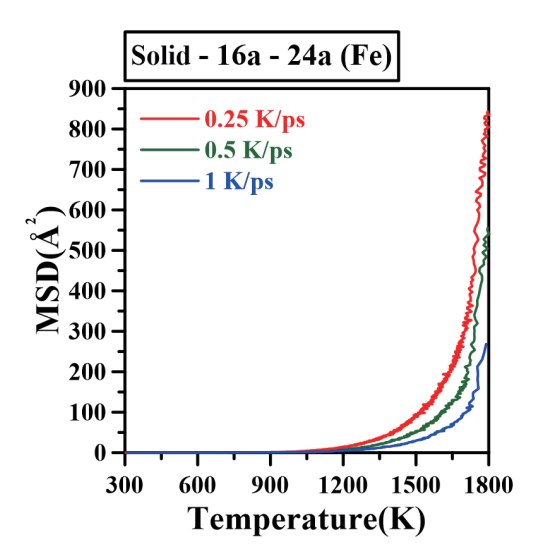
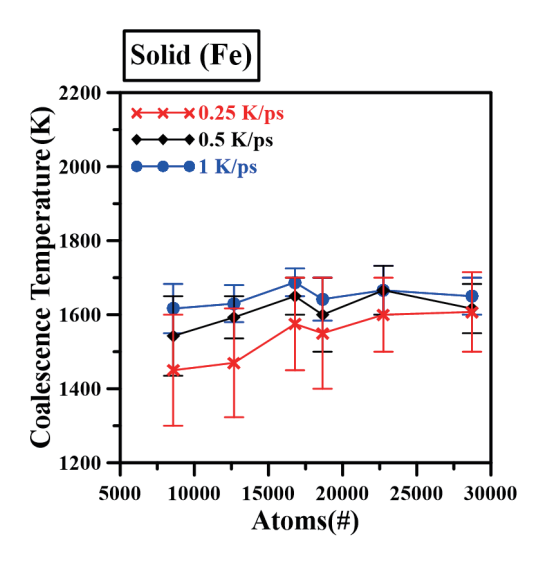
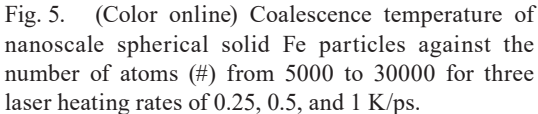


Fig. 4. (Color online) Temperature variation with MSD for nanoscale spherical solid Fe particles of the combination 16a–24a at laser heating rates of 0.25, 0.5, and 1 K/ps in the range from 300 to 1800 K.





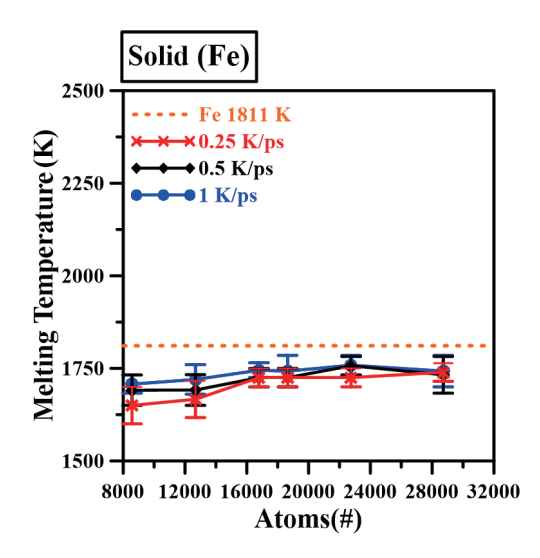


Fig. 6. (Color online) Melting temperature of nanoscale spherical solid Fe particles against the number of atoms (#) from 8000 to 32000 for three laser heating rates of 0.25, 0.5, and 1 K/ps. The red dashed line indicates the macroscopic melting point of Fe, 1811 K.

There were four substates (a), (b), (c), and (d), as shown in Fig. 7. At Point a, the initial gap of 5 Å of nanoscale spherical hollow Fe particles was maintained, R_g was 38.48 Å, the neck width was 0 Å, BCC accounted for 55.93%, HCP and FCC accounted for 0%, and other structures accounted for 44.07% of substate (a). At Point b, nanoscale spherical hollow Fe particles coalesced together owing to the small size effect. At Point b, R_g was 38.47 Å, the neck width was 21.52 Å, BCC accounted for 56.29%, HCP and FCC accounted for 0%, and other structures accounted for 43.71% of substate (b). At Point c, R_g was 38.47 Å, the neck width was 26.48 Å, BCC accounted for 55.69%, HCP and FCC accounted for 0%, and other structures accounted for 44.31% of substate (c). At Point d, R_g was 38.45 Å, the neck width was 23.06 Å, BCC accounted for 56.63%, HCP and FCC accounted for 0%, and other structures accounted for 43.37% of substate (d).

3.2.2 Sintering

For the nanoscale spherical solid Fe particles in Sect. 3.1, the results of nanoscale spherical hollow Fe particles simulated by LAMMP can be divided into four parts, as shown in Fig. 8. Figure 8 shows that the heated nanoscale spherical hollow Fe particles were divided into four sections by Points A, B, C, D, and E. From Points A to C, nanoscale spherical hollow Fe particles were comparatively stable. The coalescence stage was from Point C to Point D. The melting stage was from Point D to Point E. Beyond Point E, nanoscale spherical hollow Fe particles were completely melted.

We observed that Fig. 8 is similar to Fig. 3. The diffusion temperature starts at 1120 K and the diffusive MSD is 550 $Å^2$ at 1 K/ps in Fig. 3. In Fig. 8, the diffusion temperature starts at 980 K, and the diffusive MSD is 1100 $Å^2$ at 0.25 K/ps.

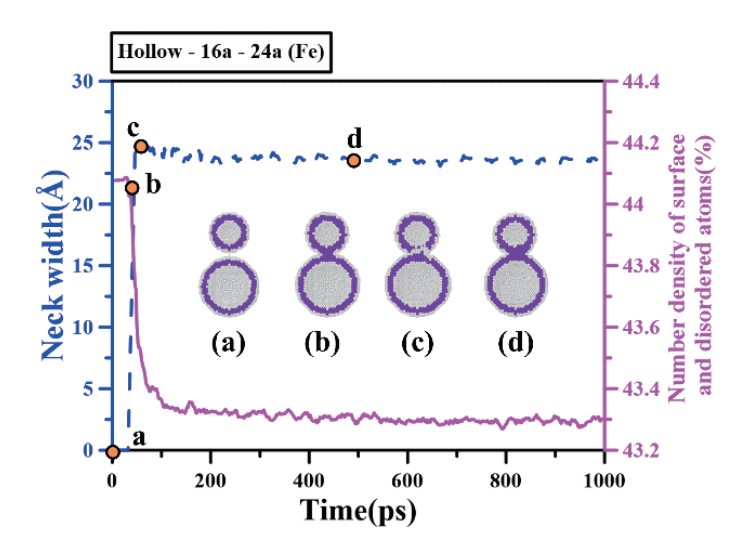


Fig. 7. (Color online) Nanoscale spherical hollow Fe particles of the combination 16a–24a in Table 1. Variations of the number density of surface and disordered Fe atoms and the neck width are plotted at different time steps at room temperature (300 K).

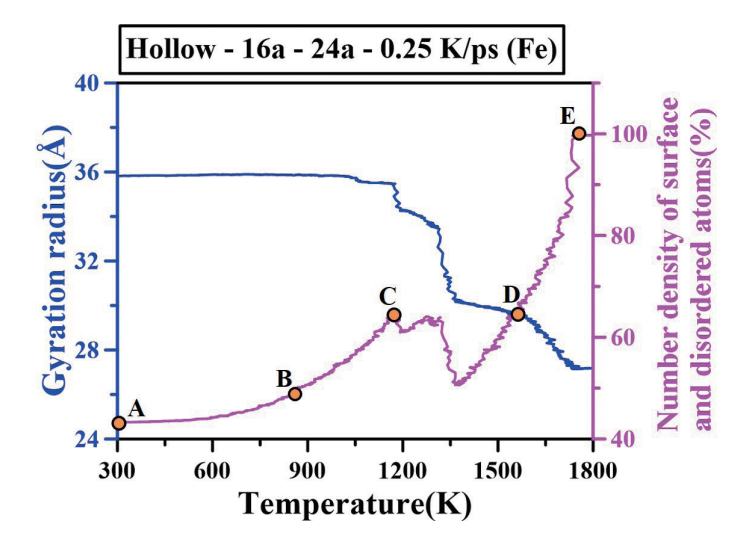


Fig. 8. (Color online) Nanoscale spherical hollow Fe particles of the combination 16a-24a in Table 1 were heated at 0.25 K/ps in the range from 300 to 1800 K. The temperature dependence of the gyration radius R_g and number density of surface and disordered atoms for the hollow Fe nanoparticle pair of 16a versus 24a with the heating rate of $0.25 \mathrm{Kps}^{-1}$ is shown.

The diffusive temperature of nanoscale spherical hollow Fe particles with identical and different particle sizes at 1 K/ps was from 1111 to 1160 K, and the diffusive MSD was from 496 to 670 Å². The diffusive temperature starting at 0.5 K/ps was from 1020 to 1080 K, and the diffusive MSD was from 750 to 865 Å². The diffusive temperature starting at 0.25 K/ps was from 932 to 1010 K, and the diffusive MSD was from 1020 to 1375 Å².

By way of R_g and the potential energy function determined from the data in Fig. 9, the coalescence temperatures of nanoscale spherical hollow Fe particles were found to be in the range from 1150 to 1682 K, as shown in Fig. 10, and the melting temperatures of nanoscale spherical hollow Fe particles were in the range from 1515 to 1767 K, as shown in Fig. 11.

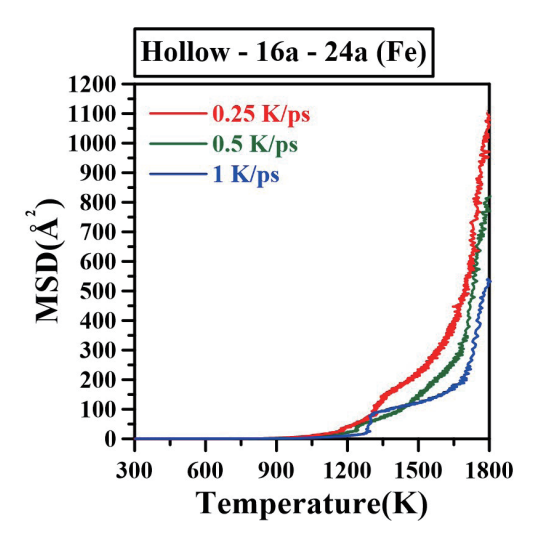
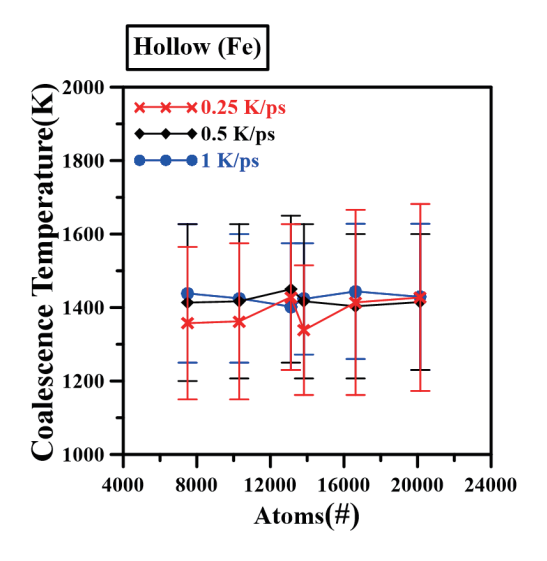


Fig. 9. (Color online) Temperature changes vs MSD of nanoscale spherical hollow Fe particles of the combination 16a–24a at three laser heating rates in the range from 300 to 1800 K.



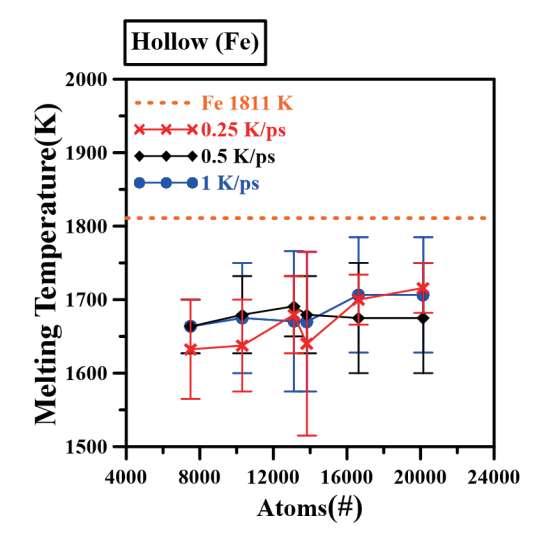


Fig. 10. (Color online) Coalescence temperatures as a function of number of Fe atoms in the range from 4000 to 24000 for nanoscale spherical hollow Fe particles heated at three laser heating rates of 0.25, 0.5, and 1 K/ps.

Fig. 11. (Color online) Melting temperature as a function of number of Fe atoms in the range from 4000 to 24000 for nanoscale spherical solid Fe particles heated at 0.25, 0.5, and 1 K/ps. The macroscopic melting point of Fe, 1811 K, is indicated by the red dashed line.

4. Conclusions

The mechanical properties of nanoscale spherical solid and hollow Fe particles of various sizes were observed at several heating rates under laser PBF AM. The laser heating rates of 0.25, 0.5, and 1 K/ps were investigated in this study and the findings are listed below.

1. Solid-state sintering can occur for the simulated Fe nanoparticles at a room temperature of 300 K. Under the sintering conditions of nanoscale spherical solid and hollow Fe particles,

- crystal defects and dislocations occurred temporarily. This was caused by the high surface-area-to-volume ratio.
- 2. Because the surface-area-to-volume ratio of nanoscale spherical hollow Fe particles is higher than that of nanoscale spherical solid Fe particles, the coalescence and melting temperatures of the nanoscale spherical hollow Fe particles are higher than those of the nanoscale spherical solid Fe particles.
- 3. The interdiffusion behavior of Fe atoms slowed down with increasing heating rate, and *vice versa*
- 4. The coalescence temperatures of nanoscale spherical solid Fe particles are in the range from 1300 to 1732 K, and those of nanoscale spherical hollow Fe particles are in the range from 1150 to 1682 K.
- 5. The melting temperatures of nanoscale spherical solid Fe particles are in the range from 1600 to 1785 K, and those of nanoscale spherical hollow Fe particles are in the range from 1515 to 1767 K.
- 6. The macroscale melting point of Fe (1811 K) is considerably higher than the melting temperatures of nanoscale spherical solid and hollow Fe particles.
- 7. The sizes and geometrical microstructures of nanoscale particles and laser heating rates are important factors during laser PBF AM.

Acknowledgments

We thank the National Computing Center of the National Institutes of Applied Research, Taiwan for their support through the provision of supercomputer resources, computing time, and facilities. We would also like to thank Yu-Wen Chiang, Yu-Sheng Lin, Chi-Wen Yang, Chao-Chen Li, Kuei-Shu Hsu, Li-Ming Chu, and Yu-Chen Su for their spiritual encouragement and academic efforts in MD simulations, data compilation, and preliminary writing of this paper.

References

- 1 I. Tomaz, S. Uí Mhurchadha, S. Marques, P. Quinn, H. Funke, F. Birkholz, S. Zietzschmann, and R. Raghavendra: Addit. Manuf. Lett. 1 (2021) 100004. https://doi.org/10.1016/j.addlet.2021.100004
- 2 J. Contreras-Naranjo, V. Perez-Gonzalez, M. Mata-Gómez, and O. Aguilar: Electrochem. Commun. 130 (2021) 107098. https://doi.org/10.1016/j.elecom.2021.107098
- 3 M. A. Obeidi, A. Conway, A. Mussatto, M. N. Dogu, S. Sreenilayam, H. Ayub, I. Ahad, and D. Brabazon: Addit Manuf. 13 (2022) 100264. https://doi.org/10.1016/j.rinma.2022.100264
- 4 A. Bacciaglia, A. Ceruti, and A. Liverani: Procedia Comput. Sci. 200 (2022) 1113. https://doi.org/10.1016/j.procs.2022.01.311
- 5 M. Binder, L. Kirchbichler, C. Seidel, C. Anstaett, G. Schlick, and G. Reinhart: Procedia CIRP. 81 (2019) 992. https://doi.org/10.1016/j.procir.2019.03.240
- 6 A. A. Foroozmehr, M. Badrossamay, E. Foroozmehr, and S. Golabi: Mater. Des. **89** (2016) 255. https://doi.org/10.1016/j.matdes.2015.10.002
- 7 R. Yavari, A. Riensche, E. Tekerek, L. Jacquemetton, H. Halliday, M. Vandever, A. Tenequer, V. Perumal, A. Kontsos, Z. Smoqi, K. Cole, and P. Rao: Mater. Des. 211 (2021) 110167. https://doi.org/10.1016/j.matdes.2021.110167
- 8 J. Jeon, S. Jiang, F. Rahmani, and S. Nouranian: J. Nanopart. Res. **22** (2020) 26. https://doi.org/10.1007/s11051-019-4747-3
- 9 A. A. Mostafaei, A. Elliott, J. Barnes, F. Li, W. Tan, C. Cramer, P. Nandwana, and M. Chmielus: Prog. Mater Sci. 119 (2021) 100707. https://doi.org/10.1016/j.pmatsci.2020.100707

- 10 S. Jiang, Y. Zhang, Y. Gan, Z. Hen, and H. Peng: J. Phys. D: Appl. Phys. 46 (2013) 33. https://doi.org/10.1088/0022-3727/46/33/335302
- 11 A. P. Thompson, H. M. Aktulga, R. Berger, D. S. Bolintineanu, W. M. Brown, P. S. Crozier, P. J. Veld, A. Kohlmeyer, S. G. Moore, T. D. Nguyen, R. Shan, M. J. Stevens, J. Tranchida, C. Trott, and S. Plimpton: Comput. Phys. Commun. 271 (2022) 108171. https://doi.org/10.1016/j.cpc.2021.108171
- 12 L. F. Lai, D. M. Lu, and J. M. Lu: Sens. Mater. **34** (2022) 3911. https://doi.org/10.18494/SAM4030
- 13 L. F. Lai, K. S. Hsu, D. M. Lu, J. M. Lu, and Y. C. Su: Sens. Mater. **36** (2024) 2005. https://doi.org/10.18494/SAM4463
- 14 L. F. Lai, Y. C. Su, C. M. Chang, K. S. Hsu, D. M. Lu, and J. M. Lu: Appl. Funct. Mater. **2** (2022) 33. https://doi.org/10.35745/afm2022v02.04.0005
- 15 Y. Guo, Z. Wang, B. Zhang, J. Teng, W. Zeng, Y. Zhao, L. Fu, D. Li, Y. Ma, W. Song, L. Liu, Z. Zhang, X. Yan, L. Wang, Y. Zhu, and X. Han: Cell Rep. Phys. Sci. 3 (2022) 100736. https://doi.org/10.1016/j.xcrp.2021.100736
- 16 J. Zhang, G. Liu, and J. Sun: Nano Mater. Sci. 2 (2020) 58. https://doi.org/10.1016/j.nanoms.2019.11.002
- 17 T. Deguchi, T. Nakahara, K. Imamura, and N. Ishida: **32** (2021) 30. https://doi.org/10.1016/j.apt.2020.11.011
- 18 M. Garrett and C. P. Race: Comput. Mater. Sci. 188 (2021) 110149. https://doi.org/10.1016/j.commatsci.2020.110149
- 19 R. Bodlos, V. Fotopoulos, J. Spitaler, A. L. Shluger, and L. Romaner: Mater. 21 (2022) 101362. https://doi.org/10.1016/j.mtla.2022.101362
- 20 R. A. Johnson: Phys. Rev. B. **37** (1988) 6121. https://doi.org/10.1103/PhysRevB.37.6121
- 21 W. Polak: Comput. Mater. Sci. 201 (2022) 110882. https://doi.org/10.1016/j.commatsci.2021.110882
- 22 K. Haydukivska, V. Blavatska, and J. Paturej: Sci. Rep. 10 (2020) 14127. https://doi.org/10.1038/s41598-020-70649-z
- 23 X. Michalet: Biophys. J. **100** (2011) 252a. https://doi.org/10.1016/j.bpj.2010.12.1593

About the Authors



Ling-Feng Lai received her B.S. and M.S. degrees from Chia Nan University of Pharmacy & Science (CNU), Taiwan, in 2015 and 2018, respectively. She is currently a Ph.D. student at Southern Taiwan University of Science and Technology. Her research interests are molecular dynamics simulation and additive manufacturing. (da71y201@stust.edu.tw)



Deng-Maw Lu was a lecturer at Southern Taiwan University of Science and Technology in Taiwan from 1985 to 1988. Since 1998, he has been a professor at Southern Taiwan University of Science and Technology. His research interests are mechanical design, nanotechnology, molecular dynamics simulation, additive manufacturing, and the history of science. (dmlu@stust.edu.tw)



Chih-Liang Chu received his Ph.D. degree from National Taiwan University, Taiwan in 2002. He is now a professor in the Department of Mechanical Engineering at Southern Taiwan University of Science and Technology (STUST), Taiwan. His current research interests are in precision metrology, optical measurement system development, nano positioning system development, precision machine design, and active vibration control technology. (cliang@stust.edu.tw)



Jian-Ming Lu is now an assistance professor in the Department of AI UAS Technology at WuFeng University (WFU), Taiwan. His research interests are in artificial intelligence, unmanned aerial vehicle, nanoscale materials, graphene, carbon nanotubes, molecular dynamics simulation, and additive manufacturing. (jmlu@wfu.edu.tw)